Quantum phase transitions in a generalized compass chain with three-site interactions

Wen-Long You,[1] Yu-Cheng Qiu,[1] and Andrzej M. Oleś[2,3]

[1]*College of Physics, Optoelectronics, and Energy, Soochow University, Suzhou, Jiangsu 215006, People's Republic of China*

[2]*Max-Planck-Institut für Festkörperforschung, Heisenbergstrasse 1, D-70569 Stuttgart, Germany*

[3]*Marian Smoluchowski Institute of Physics, Jagiellonian University, Prof. S. Łojasiewicza 11, PL-30348 Kraków, Poland*

(Received 15 March 2016; revised manuscript received 24 May 2016; published 15 June 2016)

We consider a class of one-dimensional compass models with an XYZ-YZX type of three-site exchange interaction in an external magnetic field. We present the exact solution derived by means of Jordan-Wigner transformation, and study the excitation gap, spin correlations, and establish the phase diagram. Besides the canted antiferromagnetic and polarized phases, the three-site interactions induce two distinct chiral phases, corresponding to gapless spinless-fermion systems having two or four Fermi points. We find that the z component of the scalar chirality operator can act as an order parameter for these chiral phases. We also find that the thermodynamic quantities including the Wilson ratio can characterize the liquid phases. Finally, a nontrivial magnetoelectric effect is explored, and we show that the polarization can be manipulated by the magnetic field in the absence of electric field.

DOI: 10.1103/PhysRevB.93.214417

I. INTRODUCTION

The rapid development of spin-orbital physics and quantum information in recent years motivates the search for the realizations of intrinsically frustrated orbital (or pseudospin) interactions. Such interactions lead to radically different behavior from Heisenberg SU(2) isotropic exchange, and have been in the focus of very active research in recent years. It was realized that the quantum nature of orbital degrees of freedom, which may be released by emerging spin-orbital coupling and spin-orbital entanglement, is interdisciplinary and plays a crucial role in the fields of strongly correlated electrons [1–10] and cold atoms [11–15].

The strong frustration of spin-orbital interactions can be best understood by considering generic orbital models, in which the bond-directional interactions provide the building blocks. Among them, the two-dimensional (2D) compass model defined on a square lattice [16] and the Kitaev model on a honeycomb lattice [17] can be treated as two quintessential pseudospin models, where the effective moments cannot simultaneously align to satisfy interactions with all neighbors as they favor the quantum states with distinct quantization axes. In fact, the latter model is a rare example of an interacting 2D spin model that can be rigorously solved, and was found to support gapped and gapless quantum spin liquids with emergent fractional excitations obeying non-Abelian statistics. Otherwise, exact solutions for 2D models with frustrated exchange exist only for classical Ising interactions where a phase transition at finite temperature is found [18]. Recent studies show that also for the 2D compass model a phase transition to nematic order occurs at finite but much lower temperature [19].

In low-dimensional magnetic systems collective quantum phenomena are particularly strong since the reduced dimensionality amplifies the consequences of frustrated interactions between individual spins. To probe the exotic phases resulting from bond-directional interactions, we introduced a one-dimensional (1D) generalized compass model (GCM) with antiferromagnetic exchange alternating between even and odd bonds [20]. Such a model may be realized in layered structures of transition metal oxides, with alternating exchange interactions along the bonds parallel to a and b axes along a zigzag chain in an (a,b) plane [21], optical lattices [22,23], trapped ions [24,25], and coupled photonic cavities [26,27].

On the other hand, the community focuses on two-body interactions in most systems studied, as they contribute to superexchange and are readily accessible experimentally. However, the range of the hybridization of the electron wave function will be finite in some realistic bonding geometries, and the effect of such long-range interactions must be addressed.

Recently three-site interactions received considerable attention in a somewhat diverse context [28–41]. They also occur in an effective spin model in a magnetic field obtained from a 1D plaquette orbital model by an exact transformation, with spin dimers that replace plaquettes. Indeed, they are coupled along the chain by three-spin interactions in the Hilbert space reduced by a factor of 2 per plaquette [42]. Such complex interactions between three subsequent sites essentially enrich the ground state phase diagram of the spin model and open new opportunities for underlying physics. Experimentally, it can be realized in NMR quantum simulators [43,44] or optical lattices [45]. Three-site spin interactions have been exhibited in multiferroics [46] and the magnetoelectric effect [33,39].

The purpose of this paper is to focus on a 1D GCM with three-site interactions. We show that this model is exactly solvable and explore the consequences of three-site interactions. By investigating spin correlations we identify two chiral phases and demonstrate the existence of a nontrivial magnetoelectric effect.

The organization of the paper is as follows. In Sec. II we introduce the Hamiltonian of the 1D GCM with three-site interactions in Eq. (4) and then present the procedure to solve it exactly by employing the Jordan-Wigner transformation in Sec. II B. The ground state and energy gap are retrieved. In Sec. III we use spin correlations to characterize each phase and quantum phase transitions (QPTs). The model in the magnetic field is analyzed in Sec. IV, and the complete phase diagram is obtained when the three-site interactions and magnetic fields are varied. The obtained exact solution allows us to present

the thermodynamic properties including the Wilson ratio in Sec. V. We also point out that the three-site interactions play a role in the magnetoelectric effect in Sec. VI. A final discussion and conclusions are given in Sec. VII.

II. GENERALIZED 1D COMPASS MODEL

A. The model with three-site exchange

We consider below a 1D chain of N sites with periodic boundary conditions, with GCM interactions given by

$$H_{\rm GCM}(\theta)=\sum_{i=1}^{N'}J_o\tilde{\sigma}_{2i-1}(\theta)\tilde{\sigma}_{2i}(\theta)+J_e\tilde{\sigma}_{2i}(-\theta)\tilde{\sigma}_{2i+1}(-\theta). \quad (1)$$

Here $N'=N/2$ is the number of two-site unit cells, while J_o and J_e denote the coupling strengths on odd and even bonds, respectively (below we take J_o as the unit of exchange interaction). The operator $\tilde{\sigma}_i(\theta)$ (with a tilde) is defined as a linear combination of $\{\sigma_i^x,\sigma_i^y\}$ pseudospin components (Pauli matrices),

$$\tilde{\sigma}_i(\theta)\equiv\cos(\theta/2)\sigma_i^x+\sin(\theta/2)\sigma_i^y. \quad (2)$$

These linear combinations imply that Ising-like interactions on an odd/even bond in Eq. (1) are characterized by the preferential easy axes selected by an arbitrary angle $\pm\theta/2$. With increasing angle θ, frustration gradually increases when the model Eq. (1) interpolates between the Ising model at $\theta=0$ and the quantum compass model (QCM) at $\theta=\pi/2$, in analogy to the 2D compass model [47]. The model was solved exactly and the ground state is found to have order along the easy axis as long as $\theta\neq\pi/2$, whereas it becomes a highly disordered spin-liquid ground state at $\theta=\pi/2$ [48,49]. Here we introduce the XZY-YZX type of three-site interaction in addition,

$$H_{\text{3-site}}=J^*\sum_{i=1}^{N}\left(\sigma_{i-1}^x\sigma_i^z\sigma_{i+1}^y-\sigma_{i-1}^y\sigma_i^z\sigma_{i+1}^x\right), \quad (3)$$

where J^* is its strength. Such interactions between three adjacent sites emerge as an energy current of a compass chain in the nonequilibrium steady states, as discussed in the Appendix.

The complete Hamiltonian of the 1D GCM with the three-site XZY-YZX interaction is

$$\mathcal{H}=H_{\rm GCM}+H_{\text{3-site}}. \quad (4)$$

B. Exact solution

We employ the Jordan-Wigner transformation which maps explicitly between quasispin operators and spinless fermion operators through the following relations [50]:

$$\begin{aligned}\sigma_j^z&=1-2c_j^\dagger c_j,\quad \sigma_j^y=i\sigma_j^x\sigma_j^z,\\ \sigma_j^x&=\prod_{i<j}(1-2c_i^\dagger c_i)(c_j+c_j^\dagger),\end{aligned} \quad (5)$$

where c_j and $c_j^\dagger$ are annihilation and creation operators of spinless fermions at site j which obey the standard anticommutation relations, $\{c_i,c_j\}=0$ and $\{c_i^\dagger,c_j\}=\delta_{ij}$. By substituting Eqs. (5) into Eq. (4), we arrive at a simple bilinear form of the Hamiltonian (4) in terms of spinless fermions:

$$\begin{aligned}\mathcal{H}=\sum_{i=1}^{N'}[&J_oe^{i\theta}c_{2i-1}^\dagger c_{2i}^\dagger+J_oc_{2i-1}^\dagger c_{2i}\\&+J_ee^{-i\theta}c_{2i}^\dagger c_{2i+1}^\dagger+J_ec_{2i}^\dagger c_{2i+1}\\&-2iJ^*(c_{2i-1}^\dagger c_{2i+1}+c_{2i}^\dagger c_{2i+2})+\text{H.c.}].\end{aligned} \quad (6)$$

Next discrete Fourier transformation for plural spin sites is introduced by

$$c_{2j-1}=\frac{1}{\sqrt{N'}}\sum_k e^{-ikj}a_k,\quad c_{2j}=\frac{1}{\sqrt{N'}}\sum_k e^{-ikj}b_k,$$

with discrete momenta as

$$k=\frac{n\pi}{N'},\quad n=-(N'-1),-(N'-3),\ldots,(N'-1). \quad (7)$$

The Hamiltonian takes the following form, which is suitable to introduce the Bogoliubov transformation:

$$\begin{aligned}\mathcal{H}=\sum_k[&B_ka_k^\dagger b_{-k}^\dagger+A_ka_k^\dagger b_k-A_k^*a_kb_k^\dagger-B_k^*a_kb_{-k}\\&-4J^*\sin k(a_k^\dagger a_k+b_k^\dagger b_k)],\end{aligned} \quad (8)$$

where

$$A_k=J_o+J_e+e^{ik},\quad B_k=J_oe^{i\theta}-J_ee^{i(k-\theta)}. \quad (9)$$

To diagonalize the Hamiltonian Eq. (8), we rewrite it in the Bogoliubov–de Gennes form,

$$\mathcal{H}=\sum_k\Gamma_k^\dagger\hat{M}_k\Gamma_k, \quad (10)$$

where

$$\hat{M}_k=\frac{1}{2}\begin{pmatrix}-G_k&0&S_k&P_k+Q_k\\0&-G_k&P_k-Q_k&-S_k\\S_k^*&P_k^*-Q_k^*&-G_k&0\\P_k^*+Q_k^*&-S_k^*&0&-G_k\end{pmatrix}, \quad (11)$$

and $\Gamma_k^\dagger=(a_k^\dagger,a_{-k},b_k^\dagger,b_{-k})$. In Eq. (11) the compact notation is introduced:

$$\begin{aligned}P_k&=-i(J_ee^{ik}+J_o)\sin\theta,\quad Q_k=(J_ee^{ik}-J_o)\cos\theta,\\S_k&=J_o+J_ee^{ik},\quad G_k=2J^*\sin k.\end{aligned} \quad (12)$$

The diagonalization of Hamiltonian (11) is achieved by a four-dimensional Bogoliubov transformation which connects the operators $\{a_k^\dagger,a_{-k},b_k^\dagger,b_{-k}\}$ with four kinds of quasiparticles, $\{\gamma_{k,1}^\dagger,\gamma_{k,2}^\dagger,\gamma_{k,3}^\dagger,\gamma_{k,4}^\dagger\}$,

$$\begin{pmatrix}\gamma_{k,1}^\dagger\\\gamma_{k,2}^\dagger\\\gamma_{k,3}^\dagger\\\gamma_{k,4}^\dagger\end{pmatrix}=\hat{U}_k\begin{pmatrix}a_k^\dagger\\a_{-k}\\b_k^\dagger\\b_{-k}\end{pmatrix}, \quad (13)$$

where the rows of $\hat{U}_k$ are eigenvectors of the Bogoliubov–de Gennes equations. The diagonalization is readily performed to

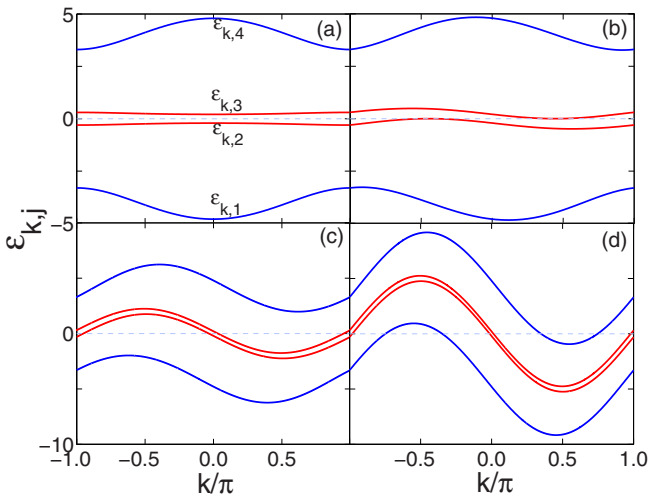

FIG. 1. The energy spectra $\varepsilon_{k,j}$ ($j = 1,\ldots,4$) for increasing J^*: (a) $J^* = 0$, (b) $J^* = 0.239$, (c) $J^* = 2$, and (d) $J^* = 5$. Parameters are as follows: $J_o = 1$, $J_e = 4$, $\theta = \pi/3$.

yield the eigenspectra $\varepsilon_{k,j}$ ($j = 1,\ldots,4$):

$$\varepsilon_{k,1(2)} = -\frac{1}{2}\Big(\sqrt{\xi_k \pm \sqrt{\xi_k^2 - \tau_k^2}} + G_k\Big),$$
$$\varepsilon_{k,3(4)} = \frac{1}{2}\Big(\sqrt{\xi_k \mp \sqrt{\xi_k^2 - \tau_k^2}} - G_k\Big), \tag{14}$$

where

$$\xi_k = |P_k|^2 + |Q_k|^2 + |S_k|^2, \quad \tau_k = \big|P_k^2 - Q_k^2 + S_k^2\big|. \tag{15}$$

The eigenenergies for various J^* are labeled sequentially from the bottom to the top as $\varepsilon_{k,1},\ldots,\varepsilon_{k,4}$ in Fig. 1. One finds that finite J^* removes the symmetry of the spectra with respect to $\varepsilon = 0$ energy and they are not invariant with respect to the $k \to -k$ transformation, in contrast to the case of the GCM with $J^* = 0$ shown in Fig. 1(a). The three-site interactions break both parity (P) symmetry and time-reversal (T) symmetry. Note that modes $k = 0, \pm\pi$ are time-reversal invariant and their excitations are independent of J^* as a consequence of vanishing G_k. Instantly, we obtain the diagonal form of the Hamiltonian,

$$\mathcal{H} = \sum_k \sum_{j=1}^{4} \varepsilon_{k,j}\gamma_{k,j}^\dagger \gamma_{k,j}. \tag{16}$$

The most important properties of the 1D quantum system can be explored in the ground state. The ground state of any fermion system follows the Fermi-Dirac statistics, and the lowest energy is obtained when all the quasiparticle states with negative energies are filled by fermions. More precisely, in the thermodynamic limit ($N \to \infty$) the ground state of the system, $|\Phi_0\rangle$, corresponds to the configuration with chemical potential $\mu = 0$, where all the states with $\varepsilon_{k,j} < 0$ are occupied and the ones with $\varepsilon_{k,j} \geqslant 0$ are empty. This state is realized by means of the corresponding occupation numbers,

$$n_{k,j} = \langle\Phi_0|\gamma_{k,j}^\dagger\gamma_{k,j}|\Phi_0\rangle = \begin{cases} 0 & \text{for } \varepsilon_{k,j} \geqslant 0, \\ 1 & \text{for } \varepsilon_{k,j} < 0. \end{cases} \tag{17}$$

One recognizes that the Bogoliubov–de Gennes Hamiltonian (11) actually acts in an artificially enlarged Nambu-spinor space and it respects an emergent particle-hole symmetry (PHS) $\mathcal{C}$, i.e., $\mathcal{C}\hat{M}_k\mathcal{C} = \hat{M}_{-k}$, with $\mathcal{C}^2 = 1$. Here in the so-called particle-hole space, the extra degree of freedom $\mathbf{C}^2$ leads to two copies of the actual excitation spectrum; a particle and a hole copy emerge simultaneously. The PHS implies here that $\gamma_{k,4}^\dagger = \gamma_{-k,1}$, $\gamma_{k,3}^\dagger = \gamma_{-k,2}$, as is evidenced in Fig. 1. The bands with positive energies correspond to the electron excitations while the negative ones are the corresponding hole excitations. When all quasiparticles above the Fermi surface are absent the ground state energy may be expressed as

$$E_0 = -\frac{1}{2}\sum_k \sum_{j=1}^{4} |\varepsilon_{k,j}|. \tag{18}$$

Accordingly, the gap is determined by the absolute value of the difference between the second and third energy branches,

$$\Delta = \min_k |\varepsilon_{k,2} - \varepsilon_{-k,3}|. \tag{19}$$

One finds that with the increase of J^*, the minimum of $\varepsilon_{k,3}$ bends down until it touches $\varepsilon = 0$ when J^* reaches a threshold value $J_{c,1}^*$, i.e., $\Delta = 0$; cf. Fig. 1(b). A gapless mode shows up at some incommensurate mode k_{ic} and the spectrum vanishes quadratically. Further increase of J^* leads to the bands' inversion between portions of $\varepsilon_{k,2}$ and $\varepsilon_{k,3}$. There is a negative-energy region of $\varepsilon_{k,3}$ in k space shown in Fig. 1(c), and there are two Fermi points across the Fermi surface. When J^* exceeds another threshold value $J_{c,2}^*$ the energy spectrum of spinless fermions may also have two additional Fermi points [31], as observed in Fig. 1(d). A Lifshitz transition occurs following the topological change of the Fermi surface in the Brillouin zone.

III. CORRELATIONS AND QUANTUM PHASE TRANSITIONS

In order to characterize the QPTs, we studied the nearest-neighbor spin correlation function defined by

$$C_l^\alpha = -\frac{2}{N}\sum_{i=1}^{N'} \langle\sigma_i^\alpha \sigma_{i+l}^\alpha\rangle, \tag{20}$$

where $l = 1$ (-1) and the superscript $\alpha = x,y,z$ denotes the Cartesian component, and the z component of scalar chirality operator [51]

$$\chi^z = -\frac{1}{N}\sum_{i=1}^{N} \langle\sigma_i^z \vec{z}\cdot[\vec{\sigma}_{i-1}\times\vec{\sigma}_{i+1}]\rangle. \tag{21}$$

The scalar chirality operator can act as a local order parameter for states without PT symmetry. As shown in Fig. 2, the ground state has finite nearest-neighbor correlation functions for $J^* = 0$, among which x components $\{C_l^x\}$ dominate for $\theta = \pi/3$, implying that the adjacent spins are antiparallel and aligned with a canted angle with respect to the x axis. Indeed, the ground state of the GCM is a canted Néel (CN) phase for $\theta < \pi/2$.

With the increase of J^*, the nearest-neighbor correlation functions remain constant. After J^* surpasses $J_{c,1}^*$, the system

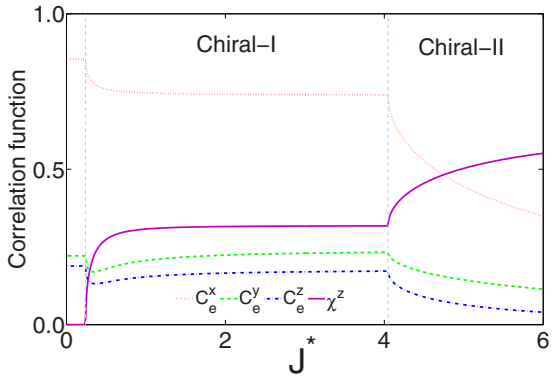

FIG. 2. The nearest-neighbor correlations C^{α} on even bonds and chirality χ^{α} by increasing J^* for $h = 0$. Parameters are as follows: $J_o = 1$, $J_e = 4$, $\theta = \pi/3$.

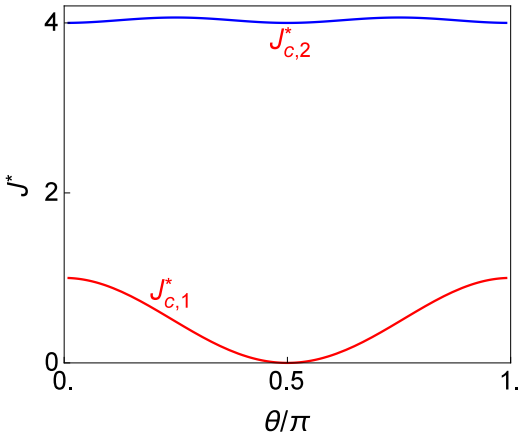

FIG. 3. The critical value of J^* as a function of θ. Parameters are as follows: $J_o = 1$, $J_e = 4$.

stays in a chiral-I phase without finite energy gap, characterized by a nonzero χ^z. In such a chiral-I phase, x components C_l^x decrease while C_l^y and C_l^z grow as J^* increases, but they become saturated quickly. When $J^* > J^*_{c,2}$, the system enters the chiral-II phase, where χ^z grows rapidly and $\{C_l^{\alpha}\}$ ($\alpha = x$, y, and z) decreases simultaneously.

In the fermionic picture different phases correspond to different Fermi-surface topology (different number of Fermi points) for fermions. In particular, the two Fermi-point spinless fermions (chiral-I phase) is distinct from the four-Fermi-point spinless fermions (chiral-II phase) [31]. Both spin-liquid phases have gapless excitations; however, the appearance of new points k_F in the Fermi surface when the controlling parameter crosses a critical value will witness a general feature of the discontinuities in the correlation functions. We remark that the number of gapless modes determine the effective central charge and the coefficients of the area-law violating term of bipartite entanglement entropy [52,53]. Notably, the chiral-II phase is a dedicated phase of the critical XX model with three-site XZY-YZX interactions added [29–34], while this phase is absent for the anisotropic XY model [38]. Here we observe that the three-site XZY-YZX interaction in the GCM surprisingly triggers both chiral states for arbitrary θ, and two different Tomonaga-Luttinger liquids reflect the importance of Fermi surface topology.

The determination of critical values of $J^*_{c,1}, J^*_{c,2}$ and the corresponding incommensurate momentum k_{ic} can be given by

$$\varepsilon_{k_{ic},3(4)} = 0, \quad \partial\varepsilon_{k_{ic},3(4)}/\partial k = 0. \tag{22}$$

This leads to the following quartic equation for $x_{ic} = \cos k_{ic}$:

$$x_{ic}^4 + c_3 x_{ic}^3 + c_2 x_{ic}^2 + c_0 = 0, \tag{23}$$

where

$$c_3 = 4\left(J_o^2 + J_e^2\right)/(3J_oJ_e\sin^2\theta),$$
$$c_2 = \left(J_o^2 + J_e^2\right)^2/\left(3J_o^2J_e^2\sin^4\theta\right) - 4\cot^4\theta/3 + 2/3,$$
$$c_0 = -1/3.$$

This quartic equation can be solved analytically but the form is rather contrived. We plot the critical lines with respect to θ in Fig. 3. One finds that in the Ising limit, i.e., for $\theta \to 0$, it yields

$$J^*_{c,1} \to \min(J_o, J_e) \quad \text{and} \quad J^*_{c,2} \to \max(J_o, J_e). \tag{24}$$

While in the compass limit, i.e., for $\theta \to \pi/2$, we have

$$J^*_{c,1} \to 0 \quad \text{and} \quad J^*_{c,2} \to \max(J_o, J_e). \tag{25}$$

In other words, the system for $\theta = \pi/2$ has an emergent $\mathbb{Z}_2$ symmetry and the ground state cannot be ordered. Any infinitesimal perturbation of J^* will induce the system into gapless chiral-I state. For the parameters we choose mostly in this paper, i.e., $J_o = 1$, $J_e = 4$, $\theta = \pi/3$, one finds $J^*_{c,1} = 0.239$ and $J^*_{c,2} = 4.048$.

IV. EFFECT OF TRANSVERSE FIELD

We now consider the case where the magnetic field h is perpendicular to the easy plane of the spins, i.e., $\vec{h} = h\hat{z}$. In this case, the Zeeman term is given by

$$\mathcal{H}_h = h\hat{z} \cdot \sum_{i=1}^{N'} (\vec{\sigma}_{2i-1} + \vec{\sigma}_{2i}), \tag{26}$$

where h is the magnitude of the transverse external field. Subsequently, in the Nambu representation, the Hamiltonian matrix $\hat{M}_k$ (11) is modified in the following way:

$$\hat{M}_k \to \hat{M}_k' = \hat{M}_k - h\mathbb{I}_2 \otimes \sigma^z, \tag{27}$$

where $\mathbb{I}_2$ is a (2×2) unity matrix. It is obvious that the external magnetic field plays the role of a chemical potential for spinless fermions.

After diagonalization four branches of energies $\varepsilon_{k,j}$, with $j = 1, \ldots, 4$, are given by the following expressions:

$$\varepsilon_{k,1(2)} = -\frac{1}{2}\left(\sqrt{\zeta_k \pm \sqrt{\eta_k}} - G_k\right),$$
$$\varepsilon_{k,3(4)} = \frac{1}{2}\left(\sqrt{\zeta_k \mp \sqrt{\eta_k}} - G_k\right), \tag{28}$$

where

$$\zeta_k = |P_k|^2 + |Q_k|^2 + |S_k|^2 + h^2,$$
$$\eta_k = (S_k^*Q_k + S_kQ_k^*)^2 - (S_k^*P_k - S_kP_k^*)^2 + (P_k^*Q_k + P_kQ_k^*)^2 + 4|S_k|^2h^2. \tag{29}$$

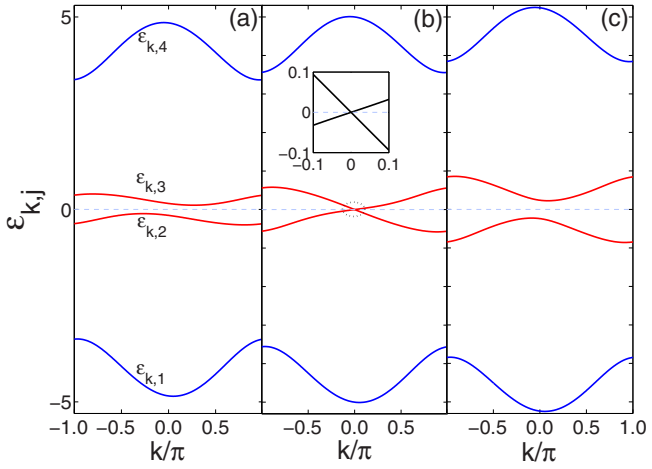

FIG. 4. The energy spectra $\varepsilon_{k,j}$ $(j = 1,\ldots,4)$ for increasing electric field h: (a) $h = 1$, (b) $h = 2$, and (c) $h = 3$. The inset in (b) is an amplification of the level crossing at the Fermi energy marked by dashed circle below. Parameters are as follows: $J_o = 1$, $J_e = 4$, $\theta = \pi/3$, and $J^* = 0.1$.

The magnetic field further breaks the T symmetry and polarizes spins along the z direction. The analytical solution for $J^* = 0$ had been scrutinized recently. One finds that increasing transverse field induces finite transverse polarization $\langle\sigma_i^z\rangle$ and drives the system into a saturated polarized phase above the critical field [20]. The field-induced QPT is of second order for arbitrary angle θ and occurs at at the critical value,

$$h_c = 2\sqrt{J_o J_e}\cos\theta. \tag{30}$$

The field-induced criticality is suited at momentum $k = 0$, where G_k does not play a role; see Eq. (12). Figure 4 shows the energy spectra obtained for three typical values of h and fixed weak $J^* = 0.1$. We find that a finite gap separates occupied from empty bands except when $h = h_c$; see Eq. (30). A small value of J^* does not modify the critical field and the gap vanishes linearly for $\theta \neq \pi/2$; see inset in Fig. 4(b). When $h = h_c$ the gap opens and grows with increasing $(h - h_c)$; see Fig. 4(c).

The nearest-neighbor correlation functions $\{C_l^\alpha\}$ $(\alpha = x, y,$ and $z)$ and the z component of scalar chirality operator χ^z for increasing J^* at $h = 3$ are shown in Fig. 5. Finite magnetic

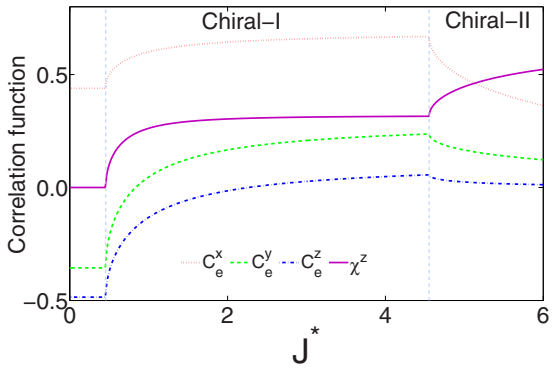

FIG. 5. The nearest-neighbor correlations C^α on even bonds and chirality χ^α by increasing J^* for $h = 3$. Parameters are as follows: $J_o = 1$, $J_e = 4$, $\theta = \pi/3$.

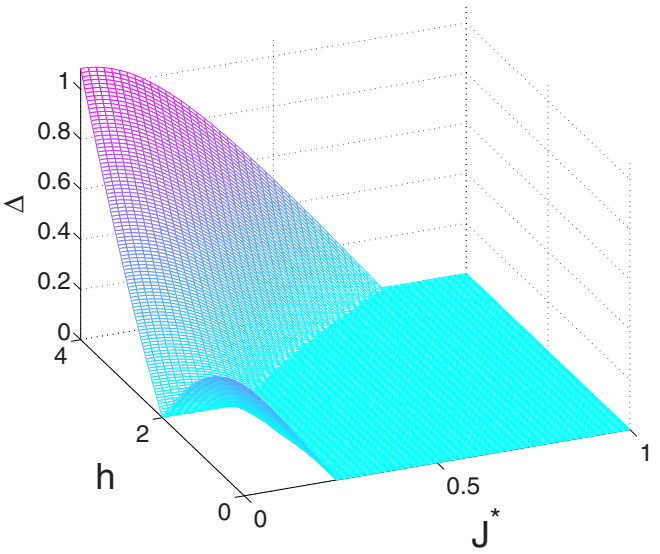

FIG. 6. The gap Δ as a function of h and J^*. Parameters are as follows: $J_o = 1$, $J_e = 4$, $\theta = \pi/3$.

field expands the range of CN phase and increases both $J_{c,1}^*$ and $J_{c,2}^*$; see Fig. 5. The z components $\{C_l^z\}$ dominate over x components $\{C_l^x\}$ for small J^* and $\theta = \pi/3$, suggesting that the spins are aligned along the z axis according to the sign of $\{C_l^z\}$. The correlation functions are found to be almost independent of J^* as long as the system is within the polarized state, but they change in a discontinuous way at phase transitions. As J^* rises above the critical value $J_{c,1}^*$, a nonzero chirality χ^z starts to grow and saturates. One finds that C_l^y and C_l^z decrease and change sign from negative to positive values upon increasing J^*, which is in contrast to the trend observed for C_l^x. A sharp upturn of χ^z occurs for $J > J_{c,2}^*$, and it continues to increase with J^*. Simultaneously, all the correlation functions $\{C_l^\alpha\}$ $(\alpha = x, y, z)$ decrease strongly towards zero when the system enters the chiral-II phase.

To present a three-dimensional panorama of the excitation gap, we display Δ for varying h and J^* in Fig. 6. The gap Δ diminishes for large value of J^*.

Similarly, we can discriminate the critical lines $J_{c,1(2)}^*$ and zero-gap modes k_{ic} using the relations in Eq. (22). The phase diagram is shown in Fig. 7. The phase diagram at finite three-site XZY-YZX interaction and magnetic field consists of four phases: (i) canted antiferromagnetic, (ii) polarized, (iii) chiral-I, and (iv) chiral-II. A tricritical point is determined by the intersection of both critical lines which can be obtained analytically:

$$h_c = 2\sqrt{J_o J_e}\cos\theta, \quad J_c^* = J_o J_e \cos^2\theta/(J_o + J_e). \tag{31}$$

In the special case of $\theta = \pi/2$, the CN phase is never stable.

V. THERMODYNAMIC PROPERTIES

Since the exact solution of the GCM with three-site interaction and the external field is at hand, it is straightforward to obtain its complete thermodynamic properties at finite temperature. All quantum phase transitions of the present 1D GCM are of second order. Among many thermodynamic quantities, the specific heat and magnetic susceptibility are

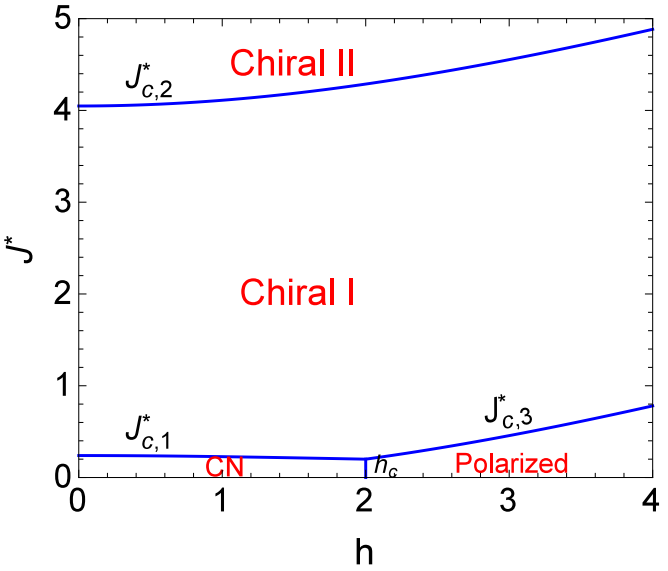

FIG. 7. Magnetic phase diagram of the 1D GCM as a function of transverse field h and three-site XZY-YXZ interaction J^*. Parameters are as follows: $J_o = 1$, $J_e = 4$, $\theta = \pi/3$.

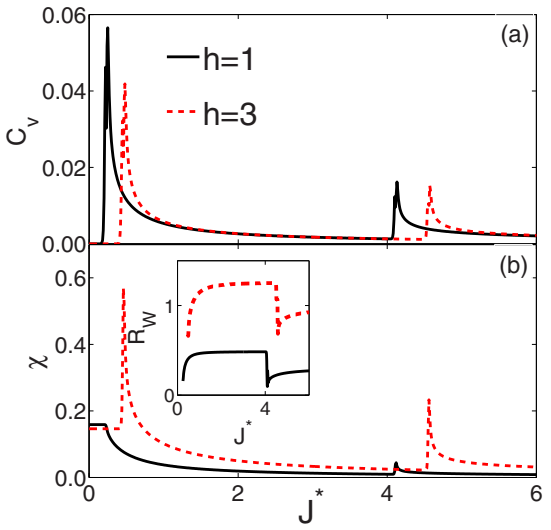

FIG. 8. The thermodynamic properties for two values of $h = 1$ and $h = 3$ at fixed temperature $T = 0.01$: (a) the specific heat C_V, (b) the magnetic susceptibility χ. The inset shows the Wilson ratio R_W (35) as a function of three-site XZY-YXZ interaction J^* for $h = 1$ and $h = 3$. Parameters are as follows: $J_o = 1$, $J_e = 4$, $\theta = \pi/3$.

easy to to be measured, and both of them are proportional to the electronic density of states at Fermi energy. For the particle-hole excitation spectrum (28), the free energy of the quantum spin chain at temperature T reads

$$\mathcal{F} = -k_B T \sum_k \sum_{j=1}^{4} \ln\left(2\cosh\frac{\varepsilon_{k,j}}{2k_B T}\right). \tag{32}$$

The low-temperature behavior of the heat capacity

$$C_V(T) = -T\left(\frac{\partial^2 \mathcal{F}}{\partial T^2}\right)_h = k_B \sum_k \sum_{j=1}^{4} \frac{(\varepsilon_{k,j}/2k_B T)^2}{\cosh^2(\varepsilon_{k,j}/2k_B T)}. \tag{33}$$

The magnetic susceptibility is defined as follows,

$$\chi(T) = -\left(\frac{\partial^2 \mathcal{F}}{\partial h^2}\right)_T - \frac{1}{2}\sum_k \sum_{j=1}^{4} \left\{ \frac{\partial^2 \varepsilon_{k,j}}{\partial h^2} \tanh\left(\frac{\varepsilon_{k,j}}{2k_B T}\right) + \left(\frac{\partial \varepsilon_{k,j}}{\partial h}\right)^2 \left[2k_B T \cosh^2\left(\frac{\varepsilon_{k,j}}{2k_B T}\right)\right]^{-1} \right\}. \tag{34}$$

At low temperatures the specific heat has a linear dependence on T in liquid metals due to the contribution from the electrons within the energy interval $k_B T$ near the Fermi surface, while the magnetic susceptibility is independent of temperature owing to the fact that only the electrons within the energy $\mu_B g H$ near the Fermi surface contribute to magnetization. The Sommerfeld-Wilson ratio (Wilson ratio in short) is a parameter which characterizes strongly correlated Fermi liquids. It is defined as a dimensionless ratio of the zero-temperature magnetic susceptibility χ and the coefficient of the linear term $\propto T$ in the electronic specific heat $C_V(T)$ [54],

$$R_W = \frac{1}{3}\left(\frac{2\pi k_B}{\mu_B g_{\text{Lande}}}\right)^2 \frac{T\chi(T)}{C_V(T)}, \tag{35}$$

where k_B is Boltzmann's constant, $\mu_B \equiv \hbar e/(2mc)$ is the Bohr magneton, and $g_{\text{Lande}} \simeq 2$ is the Lande factor. Such quantity measures the strength of magnetic fluctuations versus thermal fluctuations.

Figure 8 shows the specific heat $C_V(T)$ and the magnetic susceptibility $\chi(T)$ for increasing J^*, in the range which covers all phases. In a 1D antiferromagnet, the zero-temperature magnetic susceptibility exhibits a square-root divergence across critical fields. The Wilson ratio (35) undergoes an increase due to sudden changes in the density of states near the critical fields [55]. $R_W = 1$ in the free-electron limit when $J^* \to \infty$. However, we notice that R_W deviates from 1 in the chiral-I phase. In particular, R_W is larger here than in the chiral-II phase. Furthermore, R_W is enhanced by increasing magnetic field; see inset in Fig. 8. The Wilson ratio can be measured experimentally as for instance in a recent experiment on a gapped spin-1/2 Heisenberg ladder compound $(C_7H_{10}N)_2CuBr_2$ [56].

VI. MAGNETOELECTRIC EFFECT

Next we consider the magnetoelectric effect (MEE), where the roles of magnetization and polarization can be interchanged. A key quantity to characterize the MEE is the linear magnetoelectric susceptibility which defines the dependence of magnetization on the electric field, or the polarization dependence on the magnetic field.

The three-spin interaction was naturally claimed to contribute to the ferroelectricity in the Katsura-Nagaosa-Balatsky (KNB) formula for its particular form [57], in which the local spins (magnetic moments) and the local polarization are coupled,

$$\vec{P} = \gamma \hat{e}_{ij} \times (\vec{\sigma}_i \times \vec{\sigma}_j), \tag{36}$$

where $\hat{e}_{ij}$ is the unit vector connecting the neighboring spins $\vec{\sigma}_i$ and $\vec{\sigma}_j$ with a material-dependent coupling coefficient γ. Here we place the chain along the x direction in the real space, i.e., $\hat{e}_{ij} = (1,0,0)$. Considering a particular component (z here, to

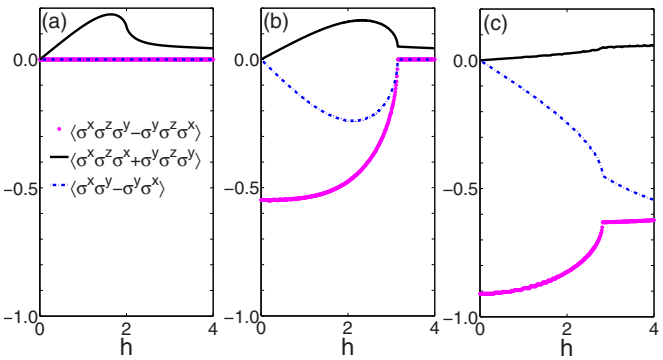

FIG. 9. Electric polarizations (see legend) as functions of external field h for (a) $J^* = 0$, (b) $J^* = 0.5$, and (c) $J^* = 4.5$. Parameters are as follows: $J_o = 1$, $J_e = 4$, $\theta = \pi/3$.

be specific) of the spin current,

$$\frac{d\sigma_l^z}{dt} = i\left[\mathcal{H}, \sigma_l^z\right] = -\mathrm{div}\, j_l^z, \tag{37}$$

which defines the current j_l^z and the corresponding P_l^y by Eq. (36).

The *electric polarization* has two sources [39]. The first term originates from the spin-current model, given by

$$P_1^y \propto \left\langle \sigma_l^x \sigma_{l+1}^y - \sigma_l^y \sigma_{l+1}^x \right\rangle, \tag{38}$$

which couples with the y component of the electric field $\vec{E}$ induced by the Dzyaloshinskii-Moriya interaction. Through the relation $\vec{P}_1 = (\partial\mathcal{H}/\partial\vec{E})$, the absence of external electric field $\vec{E}$ in Hamiltonian $\mathcal{H}$ suggests that it has little contribution to the electric polarization P_1^y. However, as shown in Fig. 9, P_1^y is induced in the presence of magnetic field h as long as the phases are chiral, and it is larger in the chiral-II phase than in the chiral-I phase.

Another contribution of electric polarization may come from the spin current triggered by the three-site interactions in the following way [39]:

$$P_2^y \propto -\left\langle \sigma_l^x \sigma_{l+1}^z \sigma_{l+2}^x + \sigma_l^y \sigma_{l+1}^z \sigma_{l+1}^y \right\rangle. \tag{39}$$

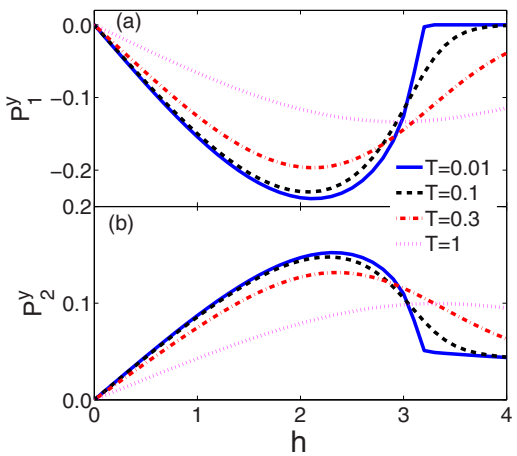

FIG. 10. The evolution of electric polarization contributions P_n^y with increasing h at different temperature T for (a) P_1^y (38), and (b) P_2^y (39). Parameters are as follows: $J_o = 1$, $J_e = 4$, $\theta = \pi/3$, $J^* = 0.5$.

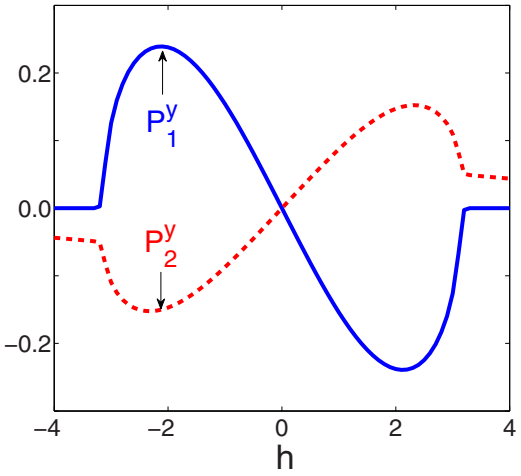

FIG. 11. The evolution of P_1^y and P_2^y by reversing the magnetic field h. Parameters are as follows: $J_o = 1$, $J_e = 4, \theta = \pi/3$, $J^* = 0.5$, $T = 0.01$.

The general form of the current operator is given in the Appendix. The form of P_2^y is the well-known XZX + YZY type of three-site interaction and remains solvable in the frame of Jordan-Wigner fermionization [29,30]. A little algebra will yield that the three-site XZX + YZY interaction acts here as a renormalization (momentum-dependent) of the magnetic field h in the Hamiltonian Eq. (27).

The manipulation of h will affect finite P_2^y in an indirect way, as is displayed in Fig. 9. We find that P_2^y is also induced by h, regardless of their phases. It has an opposite sign to P_1^y and almost complements its increase. Both P_1^y and P_2^y scale linearly with small h, indicating that they are triggered by the external magnetic field. This is in contrast to some models with two-spin interactions only, where the electric polarization can emerge only for finite electric field. The compass model with three-site interactions verifies the proposal in Ref. [58], and indeed exhibits a nontrivial magnetism-driven ferroelectricity. We can observe in Fig. 10 that the ferroelectricity phenomena are quite stable for moderate temperature. An essential feature of the ferroelectric behavior is that the electric polarization can be reversed by the reversal of the magnetic field, as is verified in Fig. 11.

VII. SUMMARY AND CONCLUSIONS

In this paper we have considered the 1D generalized compass model Eq. (4) which interpolates between the Ising model (at $\theta = 0$) and the maximally frustrated quantum compass model (at $\theta = \pi/2$) and includes three-site XZY-YZX interactions. We also investigated this model in the presence of external magnetic field. Although the system is quantum and highly frustrated, we have shown that exact solutions of the corresponding model may be obtained through Jordan-Wigner transformation.

The XZY-YZX type of three-site interactions break both the parity symmetry and the time-reversal symmetry, and then drastically modify the energy spectra, leading to two kinds of Tomonaga-Luttinger liquids. We find that moderate three-site XZY-YZX interactions will lead to a chiral-I state with two Fermi points in the representation of spinless fermions, and

large three-site XZY-YZX interactions transform the system into the four Fermi point spinless fermions. Accordingly, this modification of the Fermi surface topology follows some noticeable changes in the central charges, and then affects the ground state properties, such as nearest-neighbor correlation functions. We find that the z component of the scalar chirality operator can well distinguish gapped and gapless phases, and we also witness an abrupt change from the chiral-I to chiral-II phase. In both spin-liquid phases, not only is the magnetization influenced by the magnetic field, but the polarization emerges even for $\vec{E} = 0$ and is also affected by the magnetic field.

To conclude, we emphasize that the advantage of the model considered here is its exact solvability that implies in particular the possibility to calculate accurately various dynamic quantities. The reported results may serve to test other approximate techniques used to study more realistic models.

ACKNOWLEDGMENTS

W.-L.Y. acknowledges support by the Natural Science Foundation of Jiangsu Province of China under Grant No. BK20141190 and the NSFC under Grant No. 11474211. Y.-C.Q. acknowledges support by Hui-Chun Chin and Tsung-Dao Lee Chinese Undergraduate Research Endowment (21315003). A.M.O. kindly acknowledges support by Narodowe Centrum Nauki (NCN, National Science Center) Project No. 2012/04/A/ST3/00331.

APPENDIX: CURRENT OPERATOR FOR THE COMPASS MODEL

For a 1D compass chain, the only conserved quantity is the energy. We can decompose Eq. (1) into

$$H_{\mathrm{GCM}}(\theta) = \sum_{i=1}^{N'} h_i(\theta), \tag{A1}$$

where

$$h_i(\theta) = J_o \tilde{\sigma}_{2i-1}(\theta)\tilde{\sigma}_{2i}(\theta) + J_e \tilde{\sigma}_{2i}(-\theta)\tilde{\sigma}_{2i+1}(-\theta), \tag{A2}$$

and $\tilde{\sigma}_i(\theta)$ in defined by Eq. (2). A unit cell contains two bonds. Furthermore, one finds the commutation relations:

$$\begin{aligned}&[\tilde{\sigma}_i(\theta),\tilde{\sigma}_j(\theta)] = 0, \quad [\tilde{\sigma}_i(\theta),\tilde{\sigma}_j(-\theta)] = -2i\sin\theta\sigma_i^z\delta_{ij},\\ &[\tilde{\sigma}_i(-\theta),\tilde{\sigma}_j(\theta)] = 2i\sin\theta\sigma_i^z\delta_{ij}, \quad [\tilde{\sigma}_i(-\theta),\tilde{\sigma}_j(-\theta)] = 0.\end{aligned} \tag{A3}$$

The energy current $\hat{J}_l$ of a compass chain in the nonequilibrium steady states is calculated by taking a time derivative of the energy density and follows from the continuity equation [59,60]:

$$\begin{aligned}\frac{dh_l}{dt} &= i[\mathcal{H},h_l]\\ &= 2J_oJ_e\sin\theta\big[\tilde{\sigma}_{2l}(-\theta)\sigma_{2l+1}^z\tilde{\sigma}_{2l+2}(\theta)\\ &\quad - \tilde{\sigma}_{2l-2}(-\theta)\sigma_{2l-1}^z\tilde{\sigma}_{2l}(\theta)\big]\\ &= -(\hat{J}_{l+1} - \hat{J}_l) = -\mathrm{div}\hat{J}_l,\end{aligned} \tag{A4}$$

$$\hat{J}_l = -2J_oJ_e\sin\theta\tilde{\sigma}_{2l-2}(-\theta)\sigma_{2l-1}^z\tilde{\sigma}_{2l}(\theta). \tag{A5}$$

This energy current operator acts on three adjacent sites and has the z component of spin-1/2 operators between two odd sites. It depends on θ in general. For $\theta = 0$, it will present an XZX type, while it exhibits an XZY type for $\theta = \pi/2$ [61]. For simplicity we choose $\theta = \pi/2$ in this term while still keeping θ as an arbitrary variable in the compass chain.

Of course the odd choice of operators is artificial and follows from construction. If one defines,

$$h_l(\theta) = J_e\tilde{\sigma}_{2l}(-\theta)\tilde{\sigma}_{2l+1}(-\theta) + J_o\tilde{\sigma}_{2l+1}(\theta)\tilde{\sigma}_{2l+2}(\theta), \tag{A6}$$

to replace Eq. (A2), one finds

$$\hat{J}_l = 2J_oJ_e\sin\theta\tilde{\sigma}_{2l-1}(\theta)\sigma_{2l}^z\tilde{\sigma}_{2l+1}(-\theta). \tag{A7}$$

The above dependence proves that the "macroscopic" current, $\hat{J} = \sum_i \hat{J}_i$, will manifest itself in the presence of an effective field J^*,

$$H = H_{\mathrm{GCM}}(\theta) - J^*\sum_i \hat{J}_i. \tag{A8}$$

[1] L. F. Feiner, A. M. Oleś, and J. Zaanen, Phys. Rev. Lett. **78**, 2799 (1997); J. Phys. Condens. Matter **10**, L555 (1998).
[2] Y. Tokura and N. Nagaosa, Science **288**, 462 (2000).
[3] A. M. Oleś, G. Khaliullin, P. Horsch, and L. F. Feiner, Phys. Rev. B **72**, 214431 (2005).
[4] G. Khaliullin, Prog. Theor. Phys. Suppl. **160**, 155 (2005).
[5] A. M. Oleś, J. Phys. Condens. Matter **24**, 313201 (2012); Acta Phys. Pol. A **127**, 163 (2015).
[6] B. J. Kim, H. Ohsumi, T. Komesu, S. Sakai, T. Morita, H. Takagi, and T. Arima, Science **323**, 1329 (2009).
[7] G. Jackeli and G. Khaliullin, Phys. Rev. Lett. **102**, 017205 (2009).
[8] J. Chaloupka, G. Jackeli, and G. Khaliullin, Phys. Rev. Lett. **105**, 027204 (2010); **110**, 097204 (2013); J. Chaloupka and G. Khaliullin, Phys. Rev. B **92**, 024413 (2015).
[9] K. Wohlfeld, M. Daghofer, S. Nishimoto, G. Khaliullin, and J. van den Brink, Phys. Rev. Lett. **107**, 147201 (2011); P. Marra, K. Wohlfeld, and J. van den Brink, *ibid.* **109**, 117401 (2012); V. Bisogni, K. Wohlfeld, S. Nishimoto, C. Monney, J. Trinckauf, K. Zhou, R. Kraus, K. Koepernik, C. Sekar, V. Strocov, B. Büchner, T. Schmitt, J. van den Brink, and J. Geck, *ibid.* **114**, 096402 (2015); E. M. Plotnikova, M. Daghofer, J. van den Brink, and K. Wohlfeld, *ibid.* **116**, 106401 (2016); K. Wohlfeld, S. Nishimoto, M. W. Haverkort, and J. van den Brink, Phys. Rev. B **88**, 195138 (2013); C.-C. Chen, M. van Veenendaal, T. P. Devereaux, and K. Wohlfeld, *ibid.* **91**, 165102 (2015).
[10] W. Brzezicki, A. M. Oleś, and M. Cuoco, Phys. Rev. X **5**, 011037 (2015); W. Brzezicki, M. Cuoco, and A. M. Oleś, J. Supercond. Novel Magn. **29**, 563 (2016).
[11] E. Zhao and W. V. Liu, Phys. Rev. Lett. **100**, 160403 (2008).

[12] C. Wu, Phys. Rev. Lett. **100**, 200406 (2008); C. Wu and S. Das Sarma, Phys. Rev. B **77**, 235107 (2008).
[13] G. Sun, G. Jackeli, L. Santos, and T. Vekua, Phys. Rev. B **86**, 155159 (2012).
[14] V. Galitski and I. B. Spielman, Nature (London) **494**, 49 (2013).
[15] Z. Zhou, E. Zhao, and W. V. Liu, Phys. Rev. Lett. **114**, 100406 (2015).
[16] Z. Nussinov and J. van den Brink, Rev. Mod. Phys. **87**, 1 (2015).
[17] A. Y. Kitaev, Ann. Phys. (N.Y.) **321**, 2 (2006).
[18] L. Longa and A. M. Oleś, J. Phys. A **13**, 1031 (1980).
[19] S. Wenzel and W. Janke, Phys. Rev. B **78**, 064402 (2008); S. Wenzel, W. Janke, and A. M. Läuchli, Phys. Rev. E **81**, 066702 (2010); J. Oitmaa and C. J. Hamer, Phys. Rev. B **83**, 094437 (2011); P. Czarnik, J. Dziarmaga, and A. M. Oleś, *ibid.* **93**, 184410 (2016).
[20] W.-L. You, P. Horsch, and A. M. Oleś, Phys. Rev. B **89**, 104425 (2014).
[21] D. Xiao, W. Zhu, Y. Ran, N. Nagaosa, and S. Okamoto, Nat. Commun. **2**, 596 (2011).
[22] J. Simon, W. S. Bakr, R. Ma, M. Eric Tai, P. M. Preiss, and M. Greiner, Nature (London) **472**, 307 (2011).
[23] J. Struck, C. Ölschläger, R. Le Targat, P. Soltan-Panahi, A. Eckardt, M. Lewenstein, P. Windpassinger, and K. Sengstock, Science **333**, 996 (2011).
[24] D. Porras and J. I. Cirac, Phys. Rev. Lett. **92**, 207901 (2004).
[25] K. Kim, M. S. Chang, S. Korenblit, R. Islam, E. E. Edwards, J. K. Freericks, G. D. Lin, L. M. Duan, and C. Monroe, Nature (London) **465**, 590 (2010).
[26] M. J. Hartmann, F. G. S. L. Brandão, and M. B. Plenio, Laser Photon. Rev. **2**, 527 (2008).
[27] Z.-X. Chen, Z.-W. Zhou, X. Zhou, X.-Fa. Zhou, and G.-C. Guo, Phys. Rev. A **81**, 022303 (2010).
[28] D. Gottlieb and J. Rössler, Phys. Rev. B **60**, 9232 (1999).
[29] I. Titvinidze and G. I. Japaridze, Eur. Phys. J. B **32**, 383 (2003).
[30] V. Derzhko, O. Derzhko, and J. Richter, Phys. Rev. B **83**, 174428 (2011).
[31] P. Lou, W.-C. Wu, and M.-C. Chang, Phys. Rev. B **70**, 064405 (2004).
[32] T. Krokhmalskii, O. Derzhko, J. Stolze, and T. Verkholyak, Phys. Rev. B **77**, 174404 (2008).
[33] M. Topilko, T. Krokhmalskii, O. Derzhko, and V. Ohanyan, Eur. Phys. J. B **85**, 278 (2012).
[34] X. Liu, M. Zhong, H. Xu, and P. Tong, J. Stat. Mech. (2012) P01003.
[35] W. W. Cheng and J.-M. Liu, Phys. Rev. A **81**, 044304 (2010).
[36] Yan-Chao Li and Hai-Qing Lin, Phys. Rev. A **83**, 052323 (2011).
[37] G. Zhang and Z. Song, Phys. Rev. Lett. **115**, 177204 (2015).
[38] S. Lei and P. Tong, Physica B **463**, 1 (2015).
[39] O. Menchyshyn, V. Ohanyan, T. Verkholyak, T. Krokhmalskii, and O. Derzhko, Phys. Rev. B **92**, 184427 (2015).
[40] R. Steinigeweg, J. Gemmer, and W. Brenig, Phys. Rev. B **91**, 104404 (2015).
[41] V. Lahtinen and E. Ardonne, Phys. Rev. Lett. **115**, 237203 (2015).
[42] W. Brzezicki and A. M. Oleś, Phys. Rev. B **90**, 024433 (2014).
[43] C. H. Tseng, S. Somaroo, Y. Sharf, E. Knill, R. Laflamme, T. F. Havel, and D. G. Cory, Phys. Rev. A **61**, 012302 (1999).
[44] X. Peng, J. Zhang, J. Du, and D. Suter, Phys. Rev. Lett. **103**, 140501 (2009).
[45] J. K. Pachos and M. B. Plenio, Phys. Rev. Lett. **93**, 056402 (2004).
[46] M. Suzuki, Prog. Theor. Phys. **46**, 1337 (1971); Phys. Lett. **34**, 338 (1971).
[47] L. Cincio, J. Dziarmaga, and A. M. Oleś, Phys. Rev. B **82**, 104416 (2010).
[48] W. Brzezicki, J. Dziarmaga, and A. M. Oleś, Phys. Rev. B **75**, 134415 (2007); W. Brzezicki and A. M. Oleś, Acta Phys. Pol. A **115**, 162 (2009).
[49] W.-L. You, G.-H. Liu, P. Horsch, and A. M. Oleś, Phys. Rev. B **90**, 094413 (2014).
[50] E. Barouch and B. M. McCoy, Phys. Rev. A **2**, 1075 (1970); **3**, 786 (1971).
[51] X. G. Wen, F. Wilczek, and A. Zee, Phys. Rev. B **39**, 11413 (1989).
[52] J. Eisert, M. Cramer, and M. B. Plenio, Rev. Mod. Phys. **82**, 277 (2010).
[53] D. Eloy and J. C. Xavier, Phys. Rev. B **86**, 064421 (2012).
[54] K. Wilson, Rev. Mod. Phys. **47**, 773 (1975).
[55] X.-W. Guan, X.-G. Yin, A. Foerster, M. T. Batchelor, C.-H. Lee, and H.-Q. Lin, Phys. Rev. Lett. **111**, 130401 (2013).
[56] K. Ninios, T. Hong, T. Manabe, C. Hotta, S. N. Herringer, M. M. Turnbull, C. P. Landee, Y. Takano, and H. B. Chan, Phys. Rev. Lett. **108**, 097201 (2012).
[57] H. Katsura, N. Nagaosa, and A. V. Balatsky, Phys. Rev. Lett. **95**, 057205 (2005); M. Mostovoy, *ibid.* **96**, 067601 (2006).
[58] M. Brockmann, A. Klümper, and V. Ohanyan, Phys. Rev. B **87**, 054407 (2013).
[59] X. Zotos, F. Naef, and P. Prelovšek, Phys. Rev. B **55**, 11029 (1997).
[60] T. Antal, Z. Rácz, and L. Sasvári, Phys. Rev. Lett. **78**, 167 (1997).
[61] R. Steinigeweg and W. Brenig, arXiv:1312.4954.